^{89}Zr-Labeled Versus ^{124}I-Labeled αHER2 Fab with Optimized Plasma Half-Life for High-Contrast Tumor Imaging In Vivo

Claudia T. Mendler[1,2], Torben Gehring[1], Hans-Jürgen Wester[3], Markus Schwaiger[2], and Arne Skerra[1]

[1]Munich Center for Integrated Protein Science (CIPS-M) and Lehrstuhl für Biologische Chemie, Technische Universität München, Freising-Weihenstephan, Germany; [2]Nuklearmedizinische Klinik und Poliklinik, Klinikum Rechts der Isar, Technische Universität München, München, Germany; and [3]Pharmazeutische Radiochemie, Technische Universität München, Garching, Germany

Immuno-PET imaging of the tumor antigen HER2/neu allows for the noninvasive detection and monitoring of oncogene expression; such detection and monitoring are of prognostic value in patients with breast cancer. Compared with the full-size antibody trastuzumab, smaller protein tracers with more rapid blood clearance permit higher imaging contrast at earlier time points. Antigen-binding fragments (Fabs) of antibodies with moderately prolonged circulation achieved through the genetic fusion with a long, conformationally disordered chain of the natural amino acids Pro, Ala, and Ser (PASylation)—a biologic alternative to chemical conjugation with polyethylene glycol, PEG—offer a promising tracer format with improved pharmacokinetics for in vivo imaging. Recently, the transition metal radionuclide ^{89}Zr has attracted increasing interest for immuno-PET studies, complementing the conventional halogen radionuclide ^{124}I. **Methods:** To allow direct comparison of these 2 radioactive labels for the same protein tracer, the recombinant αHER2 Fab fused with 200 Pro, Ala, and Ser (PAS_{200}) residues was either conjugated with ^{124}I via an iodination reagent or coupled with deferoxamine (Df) and complexed with ^{89}Zr. After confirmation of the stability of both radioconjugates and quality control in vitro, immuno-PET and biodistribution studies were performed with CD1-*Foxn1^{nu}* mice bearing HER2-positive human tumor xenografts. **Results:** ^{89}Zr·Df-Fab-PAS_{200} and ^{124}I-Fab-PAS_{200} showed specific tumor uptake of 11 and 2.3 percentage injected dose per gram 24 h after injection, respectively; both led to high tumor-to-blood (3.6 and 4.4, respectively) and tumor-to-muscle (20 and 43, respectively) ratios. With regard to off-target accumulation, overt ^{124}I activity was seen in the thyroid, as expected, whereas high kidney uptake was evident for ^{89}Zr; the latter was probably due to glomerular filtration and reabsorption of the protein tracer in proximal tubular cells. **Conclusion:** Both ^{89}Zr- and ^{124}I-labeled versions of αHER2 Fab-PAS_{200} allowed PET tumor imaging with high contrast. With its residualizing radiometal, the tracer ^{89}Zr·Df-Fab-PAS_{200} showed better in vivo stability and higher tumor uptake.

Key Words: Fab; HER2; PASylation; plasma half-life; PET

J Nucl Med 2015; 56:1112–1118
DOI: 10.2967/jnumed.114.149690

Human epidermal growth factor receptor 2 (HER2/neu) is overexpressed in various cancer types, which is usually associated with an aggressive tumor phenotype as well as a poor prognosis; these features make it an important target for cancer diagnosis and therapy (*1*). Immuno-PET, with its high target specificity and spatial resolution as well as the possibility for quantitative imaging (*2*), can detect even poorly accessible HER2-positive lesions and metastases (*3*), provided that a potent HER2-specific tracer is available.

Both the halogen radionuclide ^{124}I and the transition metal radionuclide ^{89}Zr are convenient positron emitters and have been used for coupling to monoclonal antibodies in many immuno-PET studies (*4,5*). Radioiodinated proteins often show high imaging contrast, but they are less stable during both storage and application in vivo because of dehalogenation in blood plasma and tissues. Furthermore, the high positron energy of ^{124}I and the corresponding long range in tissue may reduce spatial resolution and quantification.

On the other hand, much better spatial resolution has been observed for the residualizing radionuclide ^{89}Zr because of its low average positron energy of 395 keV, which is comparable to that of ^{18}F (*6*). The availability of carrier-free ^{89}Zr produced via cyclotron irradiation of naturally abundant ^{89}Y, in conjunction with the convenient chelator deferoxamine (Df), has facilitated numerous studies with ^{89}Zr-labeled monoclonal antibodies (*7*). Df provides high selectivity for Zr(VI) and extraordinary thermodynamic stability, with a complex formation constant of greater than 10^{31} (*8*).

Indeed, the identification of HER2-positive tumor lesions was demonstrated in several studies with ^{89}Zr- or ^{111}In-labeled trastuzumab in patients with metastatic breast cancer (*9,10*). However, with regard to imaging contrast, smaller antibody fragments should be preferable over large, intact monoclonal antibodies, with their intrinsically long-lasting circulation. Conversely, smaller antigen-binding fragments (Fabs), which are prone to kidney filtration and lack FcRn-mediated endosomal recycling, promise faster tumor penetration but are rapidly cleared from blood, before sufficient accumulation in the tumor can be reached.

Recently, PASylation technology (XL-protein GmbH), which involves the genetic fusion of a biopharmaceutically active protein with a long, conformationally disordered chain of the natural amino acids Pro, Ala, and Ser (PAS), was developed as a convenient biologic alternative to PEGylation (the chemical conjugation with polyethylene glycol). PASylation offers the opportunity to easily extend the in vivo lifetime of a recombinant protein in a precise manner by expanding its hydrodynamic molecular volume and, consequently, retarding renal filtration (*11*).

Received Nov. 16, 2014; revision accepted May 12, 2015.
For correspondence or reprints contact: Arne Skerra, Lehrstuhl für Biologische Chemie, Technische Universität München, Emil-Erlenmeyer-Forum 5, 85350 Freising-Weihenstephan, Germany.
E-mail: skerra@tum.de
Published online May 21, 2015.

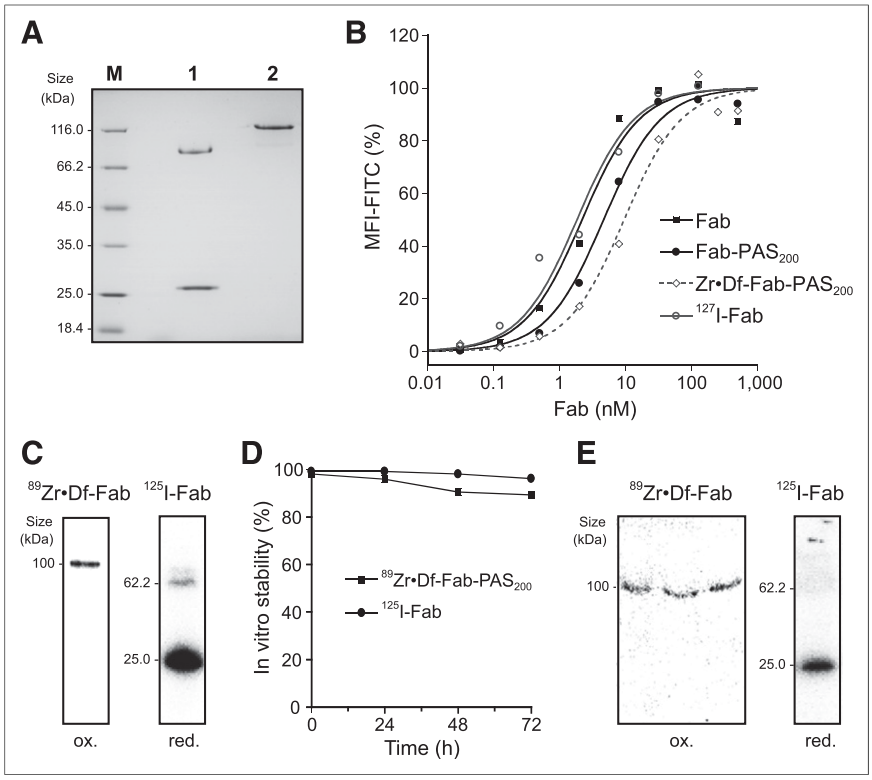

FIGURE 1. Characterization of Fab-PAS_{200}. (A) SDS-PAGE of purified Fab-PAS_{200} under reducing (lane 1) and nonreducing (lane 2) conditions. M = molecular size marker. (B) Fluorescence-activated cell sorting (FACS) titration analysis of HER2-positive cells with modified Fabs in different formats. Dissociation constants of 2.2 ± 0.6 nM for unmodified Fab, 4.7 ± 0.7 nM for Fab-PAS_{200}, 1.8 ± 0.5 for iodinated Fab (data taken from Mendler et al. (*12*)), and 9.6 ± 2.0 nM for ^{nat}Zr·Df-Fab-PAS_{200} were determined. MFI-FITC = mean fluorescence intensity of fluorescein isothiocyanate label. (C) SDS-PAGE of radiolabeled ^{89}Zr·Df-Fab-PAS_{200} under nonreducing (ox.) conditions and ^{125}I-Fab-PAS_{200} under reducing (red.) conditions. Radioactivity was detected by phosphorimaging analysis. (D) Analysis of in vitro stability of ^{89}Zr·Df-Fab-PAS_{200} and ^{125}I-Fab-PAS_{200} in phosphate-buffered saline (PBS) at various time points up to 72 h through quantification of protein-associated radioactivity by SEC and TLC. (E) Analysis of serum samples from tumor-bearing mice by SDS-PAGE and then phosphorimaging 24 h after injection with ^{89}Zr·Df-Fab-PAS_{200} or ^{125}I-Fab.

We previously applied PASylation to the trastuzumab Fab to improve its pharmacokinetic properties for PET imaging; the optimal tumor-to-blood ratio for the PAS tag was approximately 200 residues (PAS_{200}) (*12*). Here, we report on a comparison between ^{89}Zr labeling and ^{124}I labeling of the recombinant αHER2 Fab-PAS_{200} protein tracer for immuno-PET imaging of HER2-positive human xenograft tumors in mice.

MATERIALS AND METHODS

Preparation of αHER2 Fab

Recombinant protein production in *Escherichia coli* was performed as previously described (*12*). The purity, disulfide bond formation, and hydrodynamic volume were analyzed by sodium dodecyl sulfate–polyacrylamide gel electrophoresis (SDS-PAGE), size exclusion chromatography (SEC) and, finally, electrospray ionization–mass spectrometry (ESI-MS).

In Vitro Binding Studies of αHER2 Fab

The target affinity of the Fab and its derivatives on the HER2-positive human breast adenocarcinoma cell line SK-BR-3 (*13*) was determined by cytofluorimetric titration as previously described (*12*). The cells (10^5) were incubated with 100 μL of the purified Fab (or trastuzumab) at appropriate dilutions and then stained with a fluorescein-conjugated anti-human κ light-chain antibody (Invitrogen/Life Technologies). Counting was done with a FACSAria Cell-Sorting system (BD Biosciences).

Radiolabeling of Fab

A 5-fold molar excess of *p*-SCN-deferoxamine (Macrocyclics) was dissolved in dimethyl sulfoxide, and the mixture was added to a 30 μM (2 mg/mL) solution of the purified Fab in 0.1 M $NaHCO_3$ (pH 8.5) and incubated overnight at 25°C. Unconjugated chelator was removed by gel filtration on a PD-10 column (GE Healthcare) with 20 mM *N*-(2-hydroxyethyl)piperazine-*N*′-(2-ethanesulfonic acid) (HEPES)–NaOH (pH 7.0) as an eluent. Radiolabeling of the purified Df-Fab-PAS_{200} was performed in accordance with a published procedure (*14*). Typically, ^{89}Zr(IV)-oxalate (111 MBq [3 mCi]; specific activity, 150 MBq/nmol; IBA Molecular) dissolved in 1 M oxalic acid was mixed with 150 μL of water and 50 μL of 2 M Na_2CO_3, and the mixture was incubated for 3 min at room temperature (RT). After CO_2 liberation, 200 μL of 0.5 M HEPES–NaOH (pH 7.0), 75 μL of 1 M gentisic acid–NaOH (pH 7.0), and 9 nmol of the Fab in a volume of approximately 100 μL were added, and the mixture was incubated for 60 min at RT. Finally, the radiolabeled Fab was separated from free ^{89}Zr on a PD-10 column. Radiolabeling efficiency and radiochemical purity were analyzed by thin-layer chromatography (TLC) on glass microfiber chromatography paper with 20 mM sodium citrate (pH 5) as the mobile phase. For SDS-PAGE analysis and in vitro antigen-binding studies, the Fab was also labeled with nonradioactive Zr(IV) chloride (Sigma-Aldrich) dissolved in 1 M oxalic acid.

Radioiodination of Fab-PAS_{200} was performed by the IODO-GEN (Pierce) method as previously described (*12*). Generally, 0.44 nmol of the purified Fab and 37 MBq of $Na^{124}I$ (~1.1 MBq/pmol; IBA Molecular) or $Na^{125}I$ (specific activity, 74 MBq/nmol; Hartman Analytic) were incubated for 15 min at RT and the reagents were removed on a PD-10 column. Radiochemical purity was analyzed by TLC with 0.9% (w/v) NaCl as the mobile phase. The Fab labeled with nonradioactive iodide ($Na^{127}I$) under the same conditions was analyzed by SDS-PAGE and tested for antigen-binding activity.

The in vitro stability of ^{89}Zr·Df-Fab-PAS_{200} and ^{125}I-Fab-PAS_{200} in phosphate-buffered saline at RT was analyzed by TLC and SEC up to 3 d after radiolabeling. For analysis of the in vivo stability, blood samples from mice injected with the radiolabeled protein (described later) were collected 24 h after injection, and the serum was subjected to SDS-PAGE and then phosphorimaging analysis.

In Vivo Studies

For biodistribution analyses and PET imaging, female CD1-*Foxn1*^{nu} mice (Charles River Laboratories) were injected subcutaneously with 5×10^6 SK-BR-3 cells, leading to tumor sizes of 300–800 mm^3. Small-animal PET studies were performed by tail vein injection of 7 MBq of ^{89}Zr- or ^{124}I-labeled Fab-PAS_{200} ($n = 2$) with a specific activity of 11 or 80 MBq/nmol, respectively. Static maximum-intensity-projection images

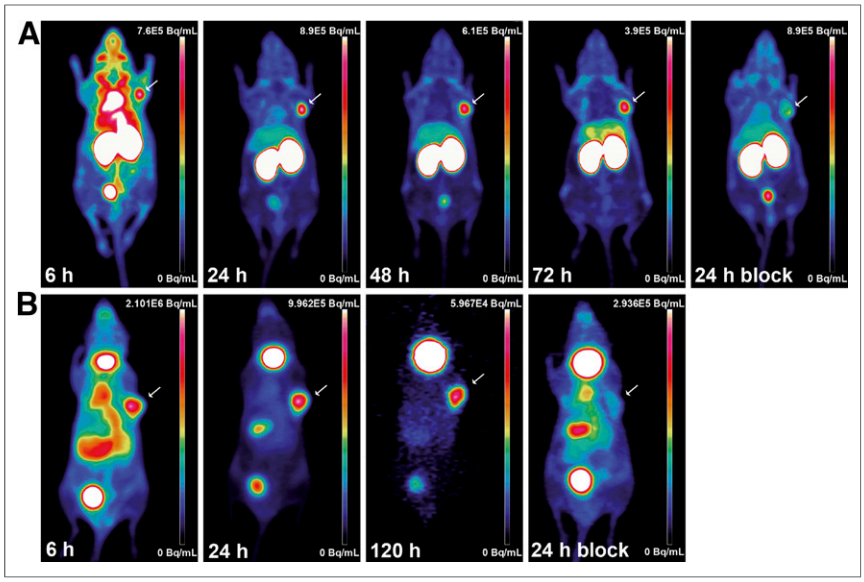

FIGURE 2. Maximum-intensity-projection PET images of xenograft tumors in mice with ^{89}Zr- and ^{124}I-labeled αHER2 Fab-PAS$_{200}$. CD1-*Foxn1*^{nu} mice bearing subcutaneous HER2-positive (SK-BR-3) human tumor xenografts at the right shoulder (arrow) were injected intravenously with 7 MBq of ^{89}Zr- or ^{124}I-labeled Fab-PAS$_{200}$. PET scans were performed for ^{89}Zr·Df-Fab-PAS$_{200}$ (A) and ^{124}I-Fab-PAS$_{200}$ (B) (the latter data taken from Mendler et al. (*12*)).

were acquired under isoflurane anesthesia with an Inveon PET/CT small-animal scanner (Siemens Medical Solutions). Quantitation of appropriate PET images (n = 1 or 2) was performed by drawing specific regions of interest in tumor and muscle tissues with Inveon software.

For biodistribution studies, mice (n = 5 or 6) were injected intravenously with 0.37–0.74 MBq each of ^{89}Zr·Df-Fab-PAS$_{200}$ and ^{125}I-Fab-PAS$_{200}$ at the same time. After 6, 24, and 48 h, blood and organs of interest were dissected and analyzed with a Wallac Wizard γ counter (PerkinElmer).

For blocking experiments (n = 5), 0.56 mg of trastuzumab from the hospital pharmacy was injected into the tail vein once 24 h before and once along with the radiolabeled Fab.

All animal experiments were approved by local authorities (Regierung von Oberbayern; license 55.2-1-54-2532-46-12) and were in compliance with regulatory and institutional guidelines.

RESULTS

Preparation of αHER2 Fab-PAS$_{200}$

For in vivo imaging of HER2-positive tumors, we applied the recombinant αHER2 Fab hu4D5v8 carrying a PAS tag of 200 residues (PAS$_{200}$) at the C terminus of the light chain to achieve a moderately extended plasma half-life (*11,12*). The Fab was produced as a functional protein through periplasmic secretion in *E. coli* and was purified in a functional state, including quantitative disulfide bridge formation between light and heavy chains, as confirmed by SDS-PAGE analysis (Fig. 1). Furthermore, SEC revealed a homogeneous peak with a decreased elution volume, indicating an expanded molecular size of the PASylated Fab, as intended.

For radiolabeling with ^{89}Zr(IV), the recombinant Fab was functionalized with the chelator reagent Df thiocyanate via Lys side chains, and ESI-MS measurements revealed a chelator-to-Fab ratio of approximately 2:1. The biochemical integrity of the Fab after conjugation was confirmed by SDS-PAGE and SEC (data not shown). The binding activity of αHER2 Fab-PAS$_{200}$ was verified by cytofluorimetric (FACS) titration analysis of the HER2-positive human tumor cell line SK-BR-3 (*13*). A dissociation constant of 2.2 nM was measured for the unmodified recombinant Fab, which is comparable to the dissociation constant of 1 nM determined for the parental antibody trastuzumab (data not shown). Generally, only a moderate influence on target affinity was seen in this assay for PASylation, Zr·Df conjugation, or iodination: 4.7 nM for Fab-PAS$_{200}$, 9.6 nM for ^{nat}Zr·Df-Fab-PAS$_{200}$, and 1.8 nM for ^{127}I-Fab (Fig. 1B).

Radioisotope Labeling

For in vivo PET imaging, αHER2 Fab-PAS$_{200}$ was separately radiolabeled with each of the positron emitters, ^{89}Zr (by Df coupling) and ^{124}I (by IODO-GEN labeling). For biodistribution experiments, ^{89}Zr- and ^{125}I-labeled proteins were applied in combination (dual tracer analysis). Radiolabeling of Df-Fab-PAS$_{200}$ with ^{89}Zr(IV)-oxalate (*14*) resulted in a labeling yield of 90%–95% after 10 min of incubation at RT, whereas iodination by the IODO-GEN method resulted in a labeling yield of 80% after 15 min of incubation at RT. With both isotopes, a radiochemical purity of greater than 98% was determined by TLC after purification on a desalting column. Tracer stability was further confirmed by SDS-PAGE analysis of the ^{89}Zr-labeled and radioiodinated Fabs (Fig. 1C).

The in vitro stability of ^{89}Zr·Df-Fab-PAS$_{200}$ (55.5 MBq/mL [1.5 mCi/mL]) in phosphate-buffered saline (PBS) at RT was investigated by SEC; after 24 and 72 h, only 2.2% and 8.9% of the bound ^{89}Zr was dissociated from the Fab, respectively (Fig. 1D). Similarly, high tracer stability of this radiometal chelate was described in other publications (*15*). In addition, tracer stability in vivo was assessed by analyzing serum collected from CD1-*Foxn1*^{nu} mice 24 h after injection of ^{89}Zr·Df-Fab-PAS$_{200}$ (described later). No signs of tracer degradation or loss of ^{89}Zr·Df were observed, and an intact disulfide bridge connecting heavy and light chains of the Fab was verified (Fig. 1E).

In Vivo PET Tumor Imaging

^{89}Zr-labeled αHER2 Fab and ^{124}I-labeled αHER2 Fab with enhanced plasma half-lives were compared for in vivo PET imaging of CD1-*Foxn1*^{nu} mice bearing subcutaneous HER2-positive human tumor xenografts. Static maximum-intensity-projection PET images were collected at appropriate time points after tracer injection (Fig. 2). Tracer specificity was confirmed in blocking experiments with an excess of unlabeled trastuzumab. For both PASylated αHER2 Fab tracers, optimal imaging contrast was observed at just 24 h after injection, with high tumor-to-normal tissue contrast and stable tumor uptake for up to several days.

However, despite similar levels of tumor staining, notable differences in the metabolization of the ^{89}Zr- and ^{124}I-labeled protein tracers became apparent. The ^{89}Zr-labeled Fab had high kidney uptake, most likely due to renal filtration of the tracer followed by reabsorption in proximal tubular cells (*16*). Although

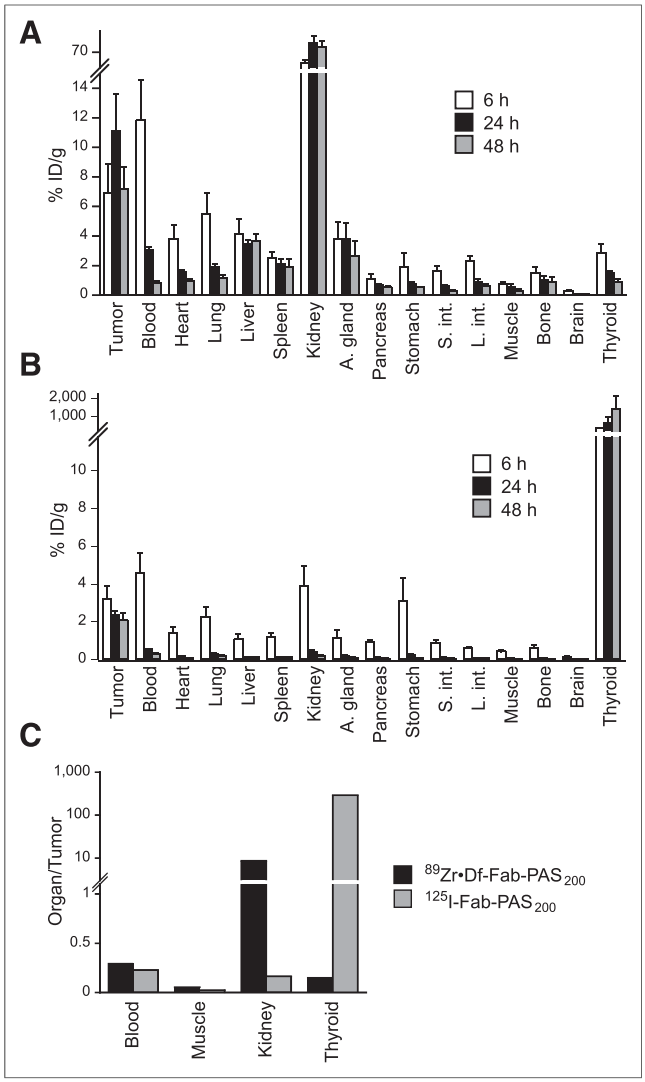

FIGURE 3. Dual tracer biodistribution analysis of ^{89}Zr- and ^{125}I-labeled αHER2 Fab-PAS$_{200}$. The biodistribution of 2 radiolabeled Fabs injected simultaneously was investigated 6, 24, and 48 h after injection. For all analyzed organs, %ID/g was plotted for ^{89}Zr·Df-Fab-PAS$_{200}$ (A) and ^{125}I-Fab-PAS$_{200}$ (B) (mean ± SD; $n = 5$). L. int. = large intestine; S. int. = small intestine. (C) Direct comparison of relevant organ-to-tumor ratios 24 h after injection for ^{125}I- and ^{89}Zr-labeled αHER2 Fab-PAS$_{200}$ (mean; $n = 5$).

^{124}I-Fab-PAS$_{200}$ probably is excreted in the same way, its degradation product (iodotyrosine), which becomes liberated after internalization and lysosomal degradation, was not trapped in this tissue. Instead, the iodide that is formed by dehalogenation accumulated in the thyroid by means of the sodium iodide symporter (*17*). Furthermore, iodide was also released from blood into the acidic gastric lumen, as indicated by enhanced radioactivity in the stomach for ^{124}I-Fab-PAS$_{200}$ (Fig. 2).

Biodistribution Studies

The in vivo imaging data were complemented by dual tracer biodistribution experiments with the PASylated αHER2 Fab labeled with either ^{89}Zr (β^+/γ) or the iodine isotope ^{125}I (γ); these tracers were injected simultaneously to avoid variations in tracer administration between animals. ^{89}Zr·Df-Fab-PAS$_{200}$ showed high tumor accumulation, with a maximum percentage injected dose per gram (%ID/g) of 11, as well as favorable tumor-to-organ ratios 24 h after injection (Fig. 3). Tracer uptake lower than the activity in blood was observed in all analyzed organs with the exception of the kidney (81 %ID/g), the adrenal gland (2.7 %ID/g), the liver (3.7 %ID/g), and the spleen (1.9 %ID/g) at later time points (48 h after injection). The fast metabolism of mice most likely was responsible for the degradation or demetalation of ^{89}Zr·Df-Fab-PAS$_{200}$ in the liver (*18*). Interestingly, no overt accumulation in bones was detected here, although this was previously observed with ^{89}Zr·Df-trastuzumab in mice (*19,20*).

When labeled with ^{125}I, Fab-PAS$_{200}$ showed prominent tumor accumulation, too, with a maximum %ID/g of 2.3 at 24 h after injection; these data revealed a high tumor-to-blood ratio of 4.4 and high tumor-to-normal tissue ratios (Table 1). With the exception of the thyroid, almost no nonspecific tracer uptake was seen in any other analyzed organ (Fig. 3B), probably because of the nonresidualizing character of this radioisotope. Finally, tracer specificity was verified in blocking experiments by injection of a 1,000-fold molar excess of trastuzumab, which resulted in 3.3-fold (^{89}Zr·Df-Fab-PAS$_{200}$) and 6.3-fold (^{125}I-Fab-PAS$_{200}$) reductions in tumor uptake ($P < 0.001$) 24 h after injection, respectively (Table 1).

Remarkably, when the 2 tracers were compared, the ^{89}Zr-labeled Fab showed total tumor uptake 24 h after injection that was 4.8-fold higher than that of the ^{125}I-labeled Fab, whereas similar tumor-to-blood ratios were observed with both radioisotopes (Fig. 3C). These findings are in line with the residualizing nature of ^{89}Zr(IV), which stays trapped inside tumor cells after receptor-mediated endocytosis and lysosomal tracer degradation (*21,22*). Notably, however, the 2 protein tracers showed different levels of nonspecific accumulation, either in the thyroid (^{125}I) or in the kidney (^{89}Zr), leading to high organ-to-tumor ratios there.

The biodistribution data were essentially in accordance with the PET experiments, in which similar uptake values in tumor and muscle for both radiolabeled αHER2 Fabs were found by quantitative image analysis (Table 2). In the liver and kidney, uptake values determined from the PET measurements approximately matched those determined from the biodistribution study. Apparent muscle activities were generally higher in PET quantification, leading to slightly decreased tumor-to-muscle ratios there.

DISCUSSION

Compared with conventional Fabs, which often show premature kidney clearance, Fabs with moderately prolonged plasma half-life enable increased tumor uptake as well as tumor-to-blood ratios (*12*). PASylation (i.e., the fusion of a protein with a conformationally disordered amino acid polymer having PEG-like properties (*11*)) can lead to improved tumor accumulation both because of the longer persistence in plasma and contact time and because of the enhanced permeability and retention effect (*23*). In contrast to PEG, the genetically encoded and biodegradable PAS tag requires no chemical modification and allows exact tuning of the desired plasma half-life. Using radioiodinated protein tracers, we previously demonstrated that a plasma half-life prolonged by approximately 4-fold (to 5.2 h) via fusion with a PAS polypeptide of 200 amino acid residues (*11*)—compared with the plasma half-life of unmodified αHER2 Fab (1.3 h)—led to favorable imaging contrast as well as tumor uptake (*12*).

TABLE 1
Biodistribution of ^{125}I- and ^{89}Zr-Labeled αHER2 Fab-PAS$_{200}$

Parameter	^{89}Zr·Df-Fab-PAS$_{200}$				^{125}I-Fab-PAS$_{200}$			
	6 h	24 h	Block (24 h)	48 h	6 h	24 h	Block (24 h)	48 h
%ID/g in tissue (mean ± SD)								
Tumor	6.89 ± 2.02	11.1 ± 1.7	3.11 ± 0.35	7.19 ± 1.46	3.21 ± 0.68	2.33 ± 0.25	0.33 ± 0.06	2.06 ± 0.40
Blood	11.8 ± 2.7	3.05 ± 0.19	2.55 ± 0.53	0.82 ± 0.13	4.56 ± 1.06	0.53 ± 0.04	0.52 ± 0.10	0.27 ± 0.05
Heart	3.79 ± 0.97	1.55 ± 0.15	1.40 ± 0.39	0.96 ± 0.14	1.38 ± 0.34	0.15 ± 0.01	0.16 ± 0.05	0.07 ± 0.01
Lung	5.50 ± 1.41	1.90 ± 0.20	1.58 ± 0.31	1.13 ± 0.23	2.25 ± 0.50	0.28 ± 0.04	0.28 ± 0.05	0.18 ± 0.05
Liver	4.11 ± 1.03	3.45 ± 0.29	2.96 ± 0.69	3.65 ± 0.48	1.06 ± 0.29	0.13 ± 0.01	0.12 ± 0.02	0.11 ± 0.02
Spleen	2.48 ± 0.41	2.10 ± 0.30	1.36 ± 0.78	1.88 ± 0.56	1.18 ± 0.22	0.12 ± 0.01	0.14 ± 0.02	0.10 ± 0.03
Kidney	49.4 ± 6.6	88.3 ± 12.8	70.7 ± 14.3	80.7 ± 10.4	3.87 ± 1.07	0.38 ± 0.09	0.34 ± 0.06	0.18 ± 0.03
Adrenal gland	3.76 ± 1.18	3.77 ± 1.12	2.26 ± 0.28	2.65 ± 0.99	1.11 ± 0.43	0.17 ± 0.03	0.16 ± 0.03	0.09 ± 0.04
Pancreas	1.06 ± 0.32	0.68 ± 0.09	0.63 ± 0.18	0.52 ± 0.09	0.90 ± 0.13	0.09 ± 0.01	0.11 ± 0.04	0.04 ± 0.01
Stomach	1.87 ± 0.95	0.76 ± 0.09	0.62 ± 0.15	0.51 ± 0.05	3.12 ± 1.22	0.21 ± 0.06	0.28 ± 0.18	0.08 ± 0.01
Small intestine	1.61 ± 0.32	0.62 ± 0.08	0.63 ± 0.17	0.29 ± 0.07	0.89 ± 0.14	0.09 ± 0.01	0.10 ± 0.02	0.04 ± 0.01
Large intestine	2.28 ± 0.38	0.91 ± 0.18	0.88 ± 0.24	0.62 ± 0.13	0.59 ± 0.09	0.08 ± 0.02	0.09 ± 0.03	0.05 ± 0.01
Muscle	0.72 ± 0.16	0.55 ± 0.23	0.47 ± 0.09	0.30 ± 0.11	0.41 ± 0.11	0.05 ± 0.02	0.06 ± 0.00	0.02 ± 0.01
Bone	1.52 ± 0.38	1.01 ± 0.27	0.84 ± 0.20	0.91 ± 0.32	0.61 ± 0.13	0.06 ± 0.01	0.07 ± 0.01	0.03 ± 0.01
Brain	0.30 ± 0.05	0.09 ± 0.01	0.07 ± 0.01	0.04 ± 0.01	0.13 ± 0.02	0.01 ± 0.00	0.01 ± 0.00	0.01 ± 0.00
Thyroid	2.88 ± 0.55	1.52 ± 0.14	1.03 ± 0.33	0.90 ± 0.17	366 ± 49	673 ± 318	461 ± 138	1412 ± 710
Ratio								
Tumor-to-blood	0.6	3.6	1.2	8.8	0.7	4.4	0.6	7.8
Tumor-to-muscle	9.6	20	6.7	24	7.8	43	5.3	101

Specific binding of this tailored Fab, labeled with either $^{124/125}$I or ^{89}Zr, to HER2-positive xenograft tumors was verified in vivo by blocking experiments with the full-size antibody trastuzumab. Both PET and biodistribution analyses showed no unfavorable accumulation in most normal tissues, indicating stable radiolabeling and confirming that modification with the biochemically inert PAS tag is compatible with in vivo imaging. In fact, remarkably clear tumor imaging contrast was seen with PET 24 h after injection. Furthermore, excellent tumor-to-blood and tumor-to-normal tissue ratios were observed in dual tracer biodistribution experiments.

Non–tumor-related tracer accumulation was detected for the ^{89}Zr-labeled Fab in the kidney, liver, and spleen and for the $^{124/125}$I-labeled Fab in the thyroid as well as stomach. This distinct radiolabel-specific behavior can be explained by the different mechanisms of in vivo demetalation and deiodination, respectively. Moreover, the kidney uptake of ^{89}Zr·Df-Fab-PAS$_{200}$ indicated that, despite an apparent molecular size above the threshold of the glomerular pores (*11*), the PASylated Fab is still excreted through renal filtration. Most likely, the protein tracer subsequently is reabsorbed in proximal tubular cells, possibly through the endocytotic, ligand-specific receptors megalin or cubulin or by means of general pinocytosis (*24*). After internalization, the labeled Fab is lysosomally catabolized into amino acids, which are released into the cytoplasm and returned to the circulation, whereas Zr·Df-lysine–peptide conjugates (or the naked metal ion) remain trapped intracellularly. Conversely, iodotyrosine, the degradation product of a radioiodinated protein, is quickly released from cells after endocytosis (by tumor cells, in the kidneys, or in other tissues) (*25*), allowing redistribution in the body.

Notably, pronounced kidney accumulation has not been observed for ^{89}Zr-labeled full-size antibodies, probably because of their extremely large molecular size and preferential clearance through the liver (*7,10*), but has been described for the ^{111}In·DOTA-conjugated αHER2 Fab (*26*). Compared with the ^{89}Zr-labeled Fab, other small protein tracers labeled with radiometals, for example, the ^{111}In-labeled αHER2 Affibody DOTA-Z$_{HER2:342\text{-}pep2}$, have shown even higher kidney uptake (>200 %ID/g) 24 h after injection—even though the participation of megalin or cubulin receptors in specific cellular uptake was excluded (*27*). On the other hand, the kidney uptake of (in terms of molecular size) the more closely related bivalent protein tracer ^{111}In·DOTA-F(ab′)$_2$-Herceptin (~65 %ID/g) 24 h after injection (*28*) was in the same range as that seen for our monovalent PASylated ^{89}Zr-labeled Fab.

To offer guidance for choosing a suitable radiolabel in the preparation of protein tracers for clinical applications, we compared the 2 different radionuclides for the labeling of αHER2 Fab-PAS$_{200}$. Direct modification of the Fab with $^{124/125}$I, a fast and easy process, did not affect target affinity and benefited from the fact that Fabs contain several accessible tyrosine residues remote from the antigen-binding site. Similar functional results were obtained for the radiometal ^{89}Zr, although conjugation with the chelator derivative Df thiocyanate to free lysine side chains of the Fab was necessary before the actual radiolabeling. Nevertheless, this modification could be performed under mild conditions as well, preserving protein integrity and target affinity. As the protein portions of both (PASylated) ^{89}Zr- and $^{124/125}$I-labeled Fabs were identical, similar behavior in vivo could be expected. Hence,

TABLE 2
Quantitation of PET Images (n = 1 or 2) for ^{124}I- and ^{89}Zr-Labeled αHER2 Fab-PAS$_{200}$

	^{89}Zr·Df-Fab-PAS$_{200}$				^{124}I-Fab-PAS$_{200}$		
Parameter	6 h	24 h	48 h	72 h	6 h	24 h	120 h
%ID/g in tissue							
Tumor	10	13	10	6.2	6.8	2.4	0.4
Muscle	1.7	0.8	0.9	0.6	0.7	0.2	0.004
Liver	9.4	7.6	5.1	3.7	3.7	1.5	0.1
Kidney	62	62	56	34	3.4	0.9	0.03
Tumor-to-muscle ratio	6.2	17	11	9.8	9.7	15.7	85

differences in the relative signals for tumor and organs, such as the kidney and liver, should be caused by different routes of metabolization for the 2 radionuclides. We purposely did not apply reagents that would block thyroid or kidney uptake (e.g., Lugol's solution, Irenat [Bayer Schering Pharma], or Gelofusine [B. Braun] (*24*)) as might be done in clinical investigations, thus allowing an unbiased comparison of tracer biodistribution.

In mouse PET experiments, the ^{124}I-labeled Fab showed relatively fast blood clearance and high tumor-to-normal tissue ratios 24 h after injection, in line with the nature of ^{124}I as a nonresidualizing radionuclide. Free iodide, which occurs after intra- or extracellular dehalogenation in blood plasma, rapidly accumulates in the thyroid because of specific import through the sodium iodide symporter (*17*). In comparison, ^{89}Zr·Df-Fab-PAS$_{200}$ had a slightly longer apparent half-time in circulation; this result could indicate higher tracer stability. Remarkably, tumor uptake that was almost 5-fold higher was observed for this label in the biodistribution analysis 24 h after injection, probably because ^{89}Zr·Df was trapped inside tumor cells after antigen binding and receptor-mediated internalization. However, despite the slightly different pharmacokinetic behavior of the 2 tracers, both essentially showed equally high tumor-to-blood ratios and high PET imaging contrast 24 h after injection.

Our observations are in line with the results of previous investigations on the differences between residualizing and nonresidualizing radiolabels. For example, a study in which different single-chain Fv-Fc fusion proteins directed against carcinoembryonic antigen (CEA) were labeled with either ^{111}In or ^{125}I revealed higher tumor uptake of the radiometal (*29*). Furthermore, experiments with the head and neck squamous cell carcinoma–selective chimeric antibody U36, labeled with either ^{89}Zr or ^{124}I, resulted in significantly higher uptake in tumor and liver for ^{89}Zr (*30*). In a similar comparison of the ^{89}Zr- and ^{124}I-labeled versions of the anti–prostate stem cell antigen minibody A11 in mice carrying prostate stem cell antigen–positive tumors, higher tumor uptake was again found for the residualizing radiometal, whereas better imaging contrast was seen for the ^{124}I-labeled minibody (*31*).

Besides biodistribution studies in mice (*20*), ^{89}Zr-labeled trastuzumab has already been tested in human patients with metastatic breast cancer (*10*), thus demonstrating potential for the noninvasive monitoring of HER2 status during cancer progression. Consequently, the clinical application of a protein tracer based on the corresponding Fab fragment should not be too difficult to achieve. Compared with ^{89}Zr-labeled full-size monoclonal antibodies, our PASylated Fab, with its optimized plasma half-life, offers the advantage of high contrast in immuno-PET imaging at just 24 h after injection. Notably, maximal contrast for ^{89}Zr·Df-Bz-SCN-trastuzumab in mice with HER2-positive BT474M1 xenografts was reached only 96–144 h after injection (*20*), in accordance with its long-lasting circulation in blood.

CONCLUSION

Depending on the chemistries of the radioisotopes, distinct in vivo distribution profiles were observed for 2 differently labeled αHER2 Fab tracers with optimized plasma half-life. ^{89}Zr-labeled Fab-PAS$_{200}$ and ^{124}I-labeled Fab-PAS$_{200}$ showed equally high tumor-to-blood ratios and high PET imaging contrast 24 h after injection. However, on the basis of the superior in vivo stability of the ^{89}Zr label and significantly higher tumor uptake overall, ^{89}Zr·Df-Fab-PAS$_{200}$ appears to be the preferred tracer for translation to clinical applications.

DISCLOSURE

The costs of publication of this article were defrayed in part by the payment of page charges. Therefore, and solely to indicate this fact, this article is hereby marked "advertisement" in accordance with 18 USC section 1734. This work was supported by ERC Grant MUMI from the European Union and Collaborative Research Centre SFB-824 of the Deutsche Forschungsgemeinschaft. Arne Skerra is a managing director and shareholder of XL-protein GmbH. No other potential conflict of interest relevant to this article was reported.

ACKNOWLEDGMENTS

We thank Dr. Calogero D'Alessandria for advice on zirconium labeling and Sybille Reder, Markus Mittelhäuser, and Marco Lehmann for performing the imaging measurements.

REFERENCES

1. Tai W, Mahato R, Cheng K. The role of HER2 in cancer therapy and targeted drug delivery. *J Control Release.* 2010;146:264–275.
2. McCabe KE, Wu AM. Positive progress in immunoPET: not just a coincidence. *Cancer Biother Radiopharm.* 2010;25:253–261.
3. Lear-Kaul KC, Yoon HR, Kleinschmidt-DeMasters BK, McGavran L, Singh M. Her-2/*neu* status in breast cancer metastases to the central nervous system. *Arch Pathol Lab Med.* 2003;127:1451–1457.
4. Börjesson PK, Jauw YW, de Bree R, et al. Radiation dosimetry of ^{89}Zr-labeled chimeric monoclonal antibody U36 as used for immuno-PET in head and neck cancer patients. *J Nucl Med.* 2009;50:1828–1836.
5. Divgi CR, Pandit-Taskar N, Jungbluth AA, et al. Preoperative characterisation of clear-cell renal carcinoma using iodine-124-labelled antibody chimeric G250 (^{124}I-cG250) and PET in patients with renal masses: a phase I trial. *Lancet Oncol.* 2007;8:304–310.
6. Disselhorst JA, Brom M, Laverman P, et al. Image-quality assessment for several positron emitters using the NEMA NU 4-2008 standards in the Siemens Inveon small-animal PET scanner. *J Nucl Med.* 2010;51:610–617.
7. Meijs WE, Haisma HJ, Klok RP, et al. Zirconium-labeled monoclonal antibodies and their distribution in tumor-bearing nude mice. *J Nucl Med.* 1997;38:112–118.
8. Severin GW, Engle JW, Barnhart TE, Nickles RJ. ^{89}Zr radiochemistry for positron emission tomography. *Med Chem.* 2011;7:389–394.
9. Perik PJ, Lub-De Hooge MN, Gietema JA, et al. Indium-111-labeled trastuzumab scintigraphy in patients with human epidermal growth factor receptor 2-positive metastatic breast cancer. *J Clin Oncol.* 2006;24:2276–2282.
10. Dijkers EC, Oude Munnink TH, Kosterink JG, et al. Biodistribution of ^{89}Zr-trastuzumab and PET imaging of HER2-positive lesions in patients with metastatic breast cancer. *Clin Pharmacol Ther.* 2010;87:586–592.

11. Schlapschy M, Binder U, Börger C, et al. PASylation: a biological alternative to PEGylation for extending the plasma half-life of pharmaceutically active proteins. *Protein Eng Des Sel.* 2013;26:489–501.
12. Mendler CT, Friedrich L, Laitinen I, et al. High contrast tumor imaging with radio-labelled antibody Fab fragments tailored for optimized pharmacokinetics via PASylation. *MAbs.* 2015;7:96–109.
13. Holmes WE, Sliwkowski MX, Akita RW, et al. Identification of heregulin, a specific activator of $p185^{erbB2}$. *Science.* 1992;256:1205–1210.
14. Vosjan MJ, Perk LR, Visser GW, et al. Conjugation and radiolabeling of monoclonal antibodies with zirconium-89 for PET imaging using the bifunctional chelate *p*-isothiocyanatobenzyl-desferrioxamine. *Nat Protoc.* 2010;5:739–743.
15. Perk LR, Vosjan MJ, Visser GW, et al. *p*-Isothiocyanatobenzyl-desferrioxamine: a new bifunctional chelate for facile radiolabeling of monoclonal antibodies with zirconium-89 for immuno-PET imaging. *Eur J Nucl Med Mol Imaging.* 2010; 37:250–259.
16. Behr TM, Goldenberg DM, Becker W. Reducing the renal uptake of radiolabeled antibody fragments and peptides for diagnosis and therapy: present status, future prospects and limitations. *Eur J Nucl Med.* 1998;25:201–212.
17. Darrouzet E, Lindenthal S, Marcellin D, Pellequer JL, Pourcher T. The sodium/iodide symporter: state of the art of its molecular characterization. *Biochim Biophys Acta.* 2014;1838:244–253.
18. Hosseinimehr SJ, Tolmachev V, Orlova A. Liver uptake of radiolabeled targeting proteins and peptides: considerations for targeting peptide conjugate design. *Drug Discov Today.* 2012;17:1224–1232.
19. Dijkers EC, Kosterink JG, Rademaker AP, et al. Development and characterization of clinical-grade ^{89}Zr-trastuzumab for HER2/*neu* immunoPET imaging. *J Nucl Med.* 2009;50:974–981.
20. Tinianow JN, Gill HS, Ogasawara A, et al. Site-specifically ^{89}Zr-labeled monoclonal antibodies for immunoPET. *Nucl Med Biol.* 2010;37:289–297.
21. Duncan JR, Behr TM, DeNardo SJ. Intracellular fate of radiometals [letter to the editor]. *J Nucl Med.* 1997;38:829.
22. Boswell CA, Marik J, Elowson MJ, et al. Enhanced tumor retention of a radiohalogen label for site-specific modification of antibodies. *J Med Chem.* 2013; 56:9418–9426.
23. Gao W, Liu W, Christensen T, Zalutsky MR, Chilkoti A. In situ growth of a PEG-like polymer from the C terminus of an intein fusion protein improves pharmacokinetics and tumor accumulation. *Proc Natl Acad Sci USA.* 2010;107:16432–16437.
24. Vegt E, de Jong M, Wetzels JF, et al. Renal toxicity of radiolabeled peptides and antibody fragments: mechanisms, impact on radionuclide therapy, and strategies for prevention. *J Nucl Med.* 2010;51:1049–1058.
25. Shih LB, Thorpe SR, Griffiths GL, et al. The processing and fate of antibodies and their radiolabels bound to the surface of tumor cells in vitro: a comparison of nine radiolabels. *J Nucl Med.* 1994;35:899–908.
26. Dennis MS, Jin H, Dugger D, et al. Imaging tumors with an albumin-binding Fab, a novel tumor-targeting agent. *Cancer Res.* 2007;67:254–261.
27. Altai M, Varasteh Z, Andersson K, Eek A, Boerman O, Orlova A. *In vivo* and *in vitro* studies on renal uptake of radiolabeled Affibody molecules for imaging of HER2 expression in tumors. *Cancer Biother Radiopharm.* 2013;28: 187–195.
28. Smith-Jones PM, Solit DB, Akhurst T, Afroze F, Rosen N, Larson SM. Imaging the pharmacodynamics of HER2 degradation in response to Hsp90 inhibitors. *Nat Biotechnol.* 2004;22:701–706.
29. Kenanova V, Olafsen T, Williams LE, et al. Radioiodinated versus radiometal-labeled anti-carcinoembryonic antigen single-chain Fv-Fc antibody fragments: optimal pharmacokinetics for therapy. *Cancer Res.* 2007;67:718–726.
30. Verel I, Visser GW, Boerman OC, et al. Long-lived positron emitters zirconium-89 and iodine-124 for scouting of therapeutic radioimmunoconjugates with PET. *Cancer Biother Radiopharm.* 2003;18:655–661.
31. Knowles SM, Zettlitz KA, Tavaré R, et al. Quantitative immunoPET of prostate cancer xenografts with ^{89}Zr- and ^{124}I-labeled anti-PSCA A11 minibody. *J Nucl Med.* 2014;55:452–459.